EI SEVIER

Contents lists available at ScienceDirect

# Water Research

journal homepage: www.elsevier.com/locate/watres



# Iron and manganese fluxes across the sediment-water interface in a drinking water reservoir



Kathryn M. Krueger <sup>a</sup>, Claire E. Vavrus <sup>a</sup>, Mary E. Lofton <sup>b</sup>, Ryan P. McClure <sup>b</sup>, Paul Gantzer <sup>c</sup>, Cayelan C. Carey <sup>b</sup>, Madeline E. Schreiber <sup>a,\*</sup>

- <sup>a</sup> Virginia Tech, Department of Geosciences, 926 W. Campus Dr, Blacksburg, VA, 24061, USA
- <sup>b</sup> Virginia Tech Department of Biological Sciences, 926 W. Campus Dr, Blacksburg, VA, 24061, USA
- <sup>c</sup> Gantzer Water Resources Engineering, 163 Rainbow Dr, Livingston, TX, 77399, USA

#### ARTICLE INFO

Article history: Received 19 November 2019 Received in revised form 29 April 2020 Accepted 30 May 2020 Available online 5 June 2020

Keywords: Anoxia Hypolimnion Metals Oxidation-reduction Redox Water-quality Hot moments

#### ABSTRACT

The development of low dissolved oxygen (DO) concentrations in the hypolimnion of drinking water reservoirs during thermal stratification can lead to the reduction of oxidized, insoluble iron (Fe) and manganese (Mn) in sediments to soluble forms, which are then released into the water column. As metals degrade drinking water quality, robust measurements of metal fluxes under changing oxygen conditions are critical for optimizing water treatment. In this study, we conducted benthic flux chamber experiments in summer 2018 to directly quantify Fe and Mn fluxes at the sediment-water interface under different DO and redox conditions of a eutrophic drinking water reservoir with an oxygenation system (Falling Creek Reservoir, Vinton, VA, USA). Throughout the experiments, we monitored DO, oxidation-reduction potential (ORP), water temperature, and pH in the chambers and compared the metal fluxes in the chambers with time-series of fluxes calculated using a hypolimnetic mass balance method. Our results showed that metal fluxes were highly variable during the monitoring period and were sensitive to redox conditions in the water column at the sediment-water interface. The time-series changes in fluxes and relationship to redox conditions are suggestive of "hot moments", short time periods of intense biogeochemical cycling. Although the metal concentrations and fluxes are specific to this site, the approaches for examining relationships between metals, oxygen concentrations and overall redox conditions can be applied by water utilities to improve water quality management of Fe and Mn. © 2020 Elsevier Ltd. All rights reserved.

#### 1. Introduction

Elevated concentrations of iron (Fe) and manganese (Mn) in drinking waters degrade water quality by affecting taste, odor, and color (USEPA, 2003). In addition, chronic exposure to elevated concentrations of Mn in drinking water has been associated with adverse health impacts, including neurological disorders in children (Bouchard et al. 2007, 2011; Khan et al., 2011; Wasserman et al., 2011). The U.S. Environmental Protection Agency (USEPA) has set secondary drinking water standards for Fe and Mn in drinking water of 0.3 and 0.05 mg L<sup>-1</sup>, respectively (USEPA, 2017). The USEPA also established a health reference level of 0.3 mg L<sup>-1</sup> for Mn (USEPA, 2003).

As both Fe and Mn are common constituents in soils, sediments and rocks, they are often found in natural waters. Fe is commonly detected in fresh water at concentrations ranging from 0.04 to 6200 mg  $\rm L^{-1}$  (Pais and Jones, 1997). Mn is also commonly detected in both surface water and groundwater worldwide, with median concentrations of 0.02 mg  $\rm L^{-1}$  and 0.05 mg  $\rm L^{-1}$ , respectively (WHO, 2008). Due to their prevalence in natural waters, Fe and Mn are commonly identified as parameters of concerns in public water systems (AWWA, 2009).

In freshwater bodies, such as lakes and reservoirs, dissolved oxygen (DO) concentrations have a strong influence on Fe and Mn dynamics (Davison, 1993). Under oxic conditions (DO > 2 mg L $^{-1}$ ), Fe and Mn occur in their oxidized, insoluble forms (e.g., Fe and Mn oxyhydroxides) in sediments. However, the development of anoxic (DO < 0.5 mg L $^{-1}$ ) conditions in the hypolimnion of many lakes and reservoirs during summer thermal stratification leads to microbial reduction of Fe and Mn in the sediments, releasing reduced, soluble

<sup>\*</sup> Corresponding author. E-mail address: mschreib@vt.edu (M.E. Schreiber).

forms of Fe and Mn into the water column (Brannon et al., 1985; Davison, 1993; De Vitre et al., 1988; Myers and Nealson, 1988).

The high cost of treating water with elevated metal concentrations, coupled with the knowledge that metals are redox-sensitive, has led many water utilities to install hypolimnetic oxygenation (HOx) systems to control metal concentrations *in situ* in lakes and reservoirs used as drinking water supplies (Bryant et al., 2011; Gantzer et al., 2009; Gerling et al., 2014). HOx systems aim to maintain thermal stratification while adding oxygen to bottom waters (Beutel and Horne, 1999). One of the goals of HOx systems is to control metal release from the sediments by introducing oxygen to the sediments and maintaining oxic hypolimnia, which helps to oxidize and precipitate soluble metals that are released into the water column (Bryant et al., 2011; Preece et al., 2019).

However, even when oxygen is added to the hypolimnion, reduced metals in sediment can still diffuse upward towards the sediment-water interface (SWI) and enter the water column (Bryant et al., 2011). At the SWI, which represents a redox boundary between the anoxic sediments and the oxic water column, reduced Fe diffusing upward is oxidized (Davison, 1993; Zaw and Chiswell, 1999). Mn behavior in freshwaters differs from that of Fe because it oxidizes more slowly and oxidation rates are controlled by pH (Davison, 1993). Thus, fluxes of reduced Mn into the overlying water column can persist even when the water column is oxic.

Designing and implementing successful HOx systems require information on the oxygen demand of the water column and the underlying sediments (Beutel, 2003; Bierlein et al., 2017; Gantzer et al., 2009; Gerling et al., 2014). Hypolimnetic oxygen demand is calculated as the rate of decrease of DO concentration in the water column of the hypolimnetic oxygen demand reflects a combination of both water column and sediment oxygen demand (SOD) (Adams et al., 1982). SOD, the consumption of DO in the sediments, contributes to the overall hypolimnetic oxygen demand (Walker and Snodgrass, 1986), making it an important parameter when designing HOx systems. For example, SOD has been estimated to be 18% and 40% of the total hypolimnetic oxygen demand in Hamilton Harbour of Lake Ontario (Polak and Haffner, 1978) and Lake Erie (Di Toro and Connolly, 1980), respectively.

Design of HOx systems also benefits from accurate measurement of metal fluxes from sediments to the water column (Adams et al., 1982), as reduced metals impart an additional (chemical) oxygen demand. Metal flux measurements are used to quantify metal loads into the water column, which are important for cost-effective treatment. In addition, measurements of metal fluxes under varying oxygen conditions are useful for constraining metal processes and cycling in freshwaters and provide important inputs into water quality models.

The goal of this study was to quantify Fe and Mn fluxes across the SWI of a drinking water reservoir under different redox conditions. To address this objective, we conducted field experiments at the reservoir using *in situ* benthic flux chambers to directly measure Fe and Mn fluxes at the SWI and compared results to hypolimnetic mass balance calculations.

#### 2. Methods

# 2.1. Site description

Falling Creek Reservoir (FCR; Fig. 1) is a small ( $Z_{max} = 9.3 \text{ m}$ , mean depth = 4 m, surface area = 0.119 km², volume =  $3.1 \times 10^5 \text{ m}^3$  at full pond), eutrophic reservoir near Vinton, Virginia, USA (Gerling et al., 2014). The reservoir is owned and operated by the Western Virginia Water Authority. FCR historically exhibits thermal stratification from May to October, which, in the absence of

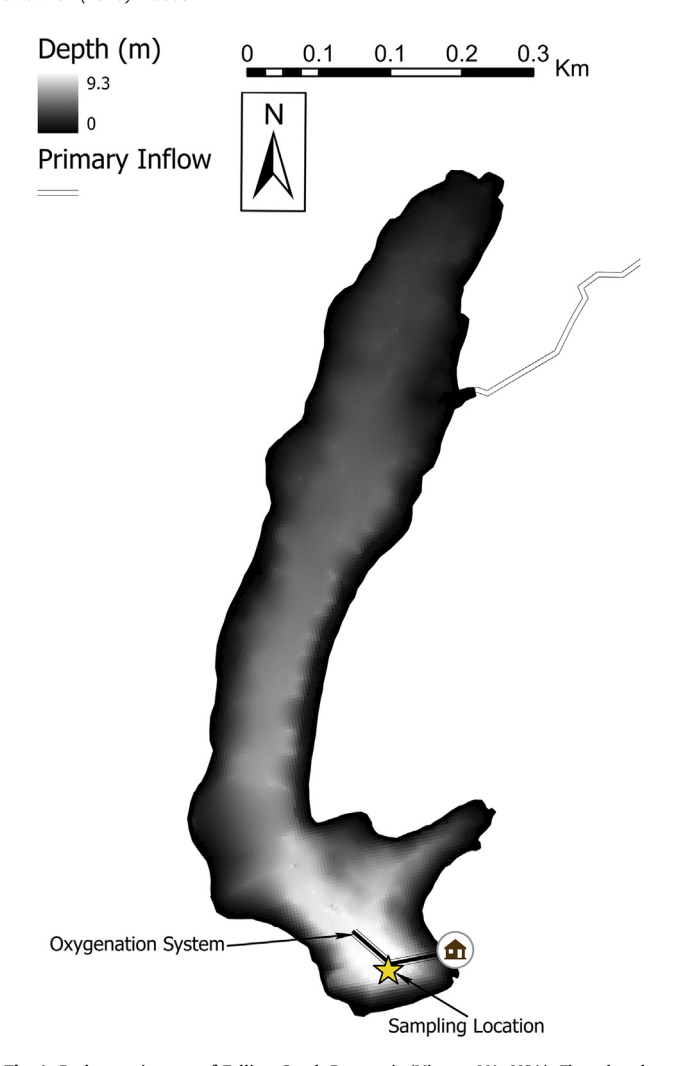


**Fig. 1.** Bathymetric map of Falling Creek Reservoir (Vinton, VA, USA). Flux chambers were deployed and water column samples were collected at the deepest site in the reservoir. Locations of the oxygenation system and the primary inflow to the reservoir are also shown.

hypolimnetic oxygenation, leads to the development of anoxic conditions in the hypolimnion (Gerling et al., 2014; Munger et al., 2016). Inflow from the upstream tributary is the largest surface water input (>90%) to the reservoir (Gerling et al., 2016).

In September 2012, a side-stream supersaturation hypolimnetic oxygenation system (HOx) was installed in FCR to increase DO concentrations in the hypolimnion of the reservoir while maintaining thermal stratification (see Gerling et al., 2014 for details on the HOx system). The HOx system consists of a submersible pump (at 8.5 m depth), inlet piping, an oxygen source, an oxygen contact chamber, and distribution headers (at 8.5 m depth). Water is withdrawn from the reservoir via the pump, transferred to the oxygen contact chamber and supersaturated with oxygen. The water is then transported to the distribution headers via the outlet piping, where it is injected back into the hypolimnion. Previous work (Gerling et al., 2014) and continued oxygen monitoring (Carey et al., 2019) demonstrate that during operation, the HOx system introduces oxygen into the hypolimnion while maintaining thermal stratification.

In 2018, when this study was conducted, the HOx system was operating at full capacity (Table 1) from April 24 to July 19. After July 19, the HOx system operated either at reduced capacity (July 19–30; August 9-September 10) or was deactivated (July 30-August

**Table 1**FCR HOx operation dates and mean volume weighted hypolimnetic DO concentration during 2018 season.

Date range in 2018	HOx system status	Mean volume-weighted hypolimnetic DO (mg/L $\pm$ S.D.)				
Apr 24 – Jul 19	ON	$4.7 \pm 0.3$				
Jul 19 – Jul 30	ON*	1.8				
Jul 30 – Aug 9	OFF	0.5				
Aug 9 – Sep 10	ON*	$0.3 \pm 0.5$				
Sep 10 - Oct 21	OFF	$0.2 \pm 0.4$				
Oct 21	Turnover (TO)	N/A				

<sup>\*</sup> operation at reduced capacity

9; September 10 on). The reservoir exhibited fall turnover (TO) and onset of isothermal conditions on October 21.

#### 2.2. Water column sampling

We collected water samples from FCR for total and soluble Fe and Mn concentrations weekly from May to October 2018 and monthly from November 2018 to April 2019. Water samples were collected at 0.1, 1.6, 3.8, 5.0, 8.0, 9.0 m depths using a 4-L Van Dorn sampler. These depths correspond to withdrawal elevations on the water treatment outlet structure near the deepest site in FCR (Fig. 1). Unfiltered samples (for analysis of operationally-defined total metals) were collected into 15 mL centrifuge tubes. Filtered samples (0.45 µm nylon membrane) were collected for analysis of soluble metals (Munger et al., 2016). We recognize that this method of filtration does not remove all particulates, so use of the term soluble is operationally-defined for the purposes of this study. Total and soluble samples for metal analysis were preserved using 0.5 mL trace metal grade nitric acid to pH < 2. Samples were analyzed for Fe and Mn concentrations using an Inductively Coupled Plasma Atomic Emission Spectrometer (ICP-AES, Spectro ARCOS) following EPA Method 200.7 (USEPA, 1994). Detection limits were  $0.004 \text{ mg L}^{-1}$  for Fe and  $0.001 \text{ mg L}^{-1}$  for Mn.

Depth profiles were measured at 0.1 m increments twice per week from the deepest site using a Seabird Electronics SBE 19plus V2 high-resolution profiler (CTD) with an SBE 43 DO probe and an SBE 27 pH/ORP probe to measure DO, temperature, pH, conductivity and ORP (Carey et al., 2019). Previous work by Gerling et al. (2014), supported by continued CTD data collection (Carey et al., 2019), showed that DO concentrations measured at the deepest site in the reservoir were representative of hypolimnetic conditions throughout the reservoir. We used temperature data to calculate the thermocline depth, which defined the upper boundary of the hypolimnion, using the MATLAB Lake Analyzer program (Read et al., 2011).

#### 2.3. Sediment sampling and analysis

Sediment samples were collected at the sediment-water interface in summer 2018 using an Ekman sampler at six locations within 150 m of the location of the benthic flux chambers. In the laboratory, sediment samples were oven-dried (95  $^{\circ}$ C) for ~96 h. To digest the samples, 10 mL of trace metal grade nitric acid was added to 0.5 g of dried sediment; the samples were then microwave-digested (CEM Mars Express) following EPA Method 3051A (USEPA, 2007). We analyzed the resulting digestion solution for Fe and Mn using ICP-MS (Thermo-Electron X-Series).

Powder X-ray diffraction (XRD) was used to examine mineralogy of five of the six samples collected. Samples were powdered using a mortar and pestle. XRD analyses were conducted using a Rigaku Mini-Flex II Desktop X-ray Diffractometer. Copper Kα

radiation was used with a fixed tubed output voltage of 30 kV and fixed tube output current of 15 mA. XRD patterns were analyzed to match peaks to known minerals.

#### 2.4. Measuring benthic fluxes

Metal fluxes across the SWI were measured using two methods: benthic flux chambers and a hypolimnetic mass balance method. The flux chambers were deployed at the deepest site to make direct measurements of Fe and Mn fluxes and oxygen demand at the SWI at two time intervals (June 21-July 2 and August 13—23). The mass balance method used measurements of discharge and metal concentrations in the hypolimnion to indirectly estimate the net release of Fe and Mn from the sediments into the hypolimnion, following the methods described by Gerling et al. (2016).

#### 2.4.1. Benthic flux chambers

To measure metal fluxes *in-situ* at the SWI, benthic flux chambers, similar to those described and deployed by Murphy and Hicks (1986) and Hicks (1990) and further modified for this study, were deployed in triplicate at the deepest site in FCR. Flux chambers capture diffusive fluxes of solutes across the SWI and have been utilized to measure fluxes of oxygen, nutrients and contaminants in a variety of coastal/marine settings and in freshwater bodies (Frogner-Kockum et al., 2016; Pakhomova et al., 2007; Tengberg et al., 2005).

For this study, we conducted two ten-day experiments in 2018 (June 21 - July 2 and August 13–23) to examine the effects of different initial DO conditions on metal fluxes. During the June experiment, hypolimnetic DO concentrations were high (7 mg L $^{-1}$ , ~71% saturation). During the August experiment, DO concentrations in the hypolimnion were substantially lower (2 mg L $^{-1}$ , ~18% saturation). Average temperature was 1 °C higher in the hypolimnion in August than it was in June.

The flux chambers used for this study isolated 24 cm of hypolimnetic water above the sediments and 0.27 m<sup>2</sup> of the SWI, for a total volume of 64.86 L of hypolimnetic water enclosed within the chambers (for diagrams of the flux chamber, see Figs. S1 and S2). Each chamber was connected to a circulation pump, which promotes circulation of the water within the chamber so that measured concentrations are representative of the entire chamber volume (Tengberg et al., 2005). The pump was fitted with a valve and sampling tubing on the outlet to collect water samples from the chambers during the incubation period. To allow for highfrequency monitoring of field parameters, each chamber contained an InsiteIG (Slidell, LA) Model 31 fluorescent DO sensor to measure temperature and DO. Comparison of DO data collected from replicate chamber experiments indicated a mean percent difference of 2%. In addition to DO sensors, one chamber contained two additional sensors, an InsiteIG model M51 pH and an InsiteIG model M52 ORP sensor (Slidell, LA). All sensors were connected to a GWR master data logger (Gantzer Water, Livingston, TX) and programmed to collect data at a 2-min interval.

The flux chambers were deployed from a boat by slowly lowering them through the water column to the bottom to minimize sediment disturbance. Once the chambers were seated on the bottom, they were flushed with hypolimnion water for 90–120 min until chamber DO concentrations and temperature stabilized and reflected the surrounding hypolimnetic conditions.

After flushing, the chambers were allowed to incubate and then checked after 24 h. Proper sealing of the chamber was verified by analyzing the linear regression of the DO data as oxygen depleted over time, where an R<sup>2</sup> of 0.99 or better indicated proper sealing. If the chamber was not properly sealed, which happened in one chamber the start of the August experiment, we lifted the chamber off the sediments, re-deployed it in a nearby location, and restarted the flushing and incubation processes.

In addition to the triplicate flux chambers, we also deployed one "water column" chamber, which had the same construction specifications as the flux chambers but had a bottom plate to seal off the chamber. This chamber was deployed to account for changes in metal concentrations within the water column that were not associated with fluxes across the SWI. This chamber was deployed for the same interval as the flux chambers in the second experiment.

During the two 10-day deployments, we collected samples for total and soluble Fe and Mn every 3–4 days. To sample the chamber, we turned the pump on and allowed water to circulate through the chamber and tubing for 1 min; we then collected 15 mL of unfiltered water for total metals analysis and an additional 15 mL of filtered (0.45  $\mu m$ ) water for soluble metals analysis. During both experiments, a maximum of 100 mL of chamber water was withdrawn at each sampling event to minimize the effects of removing chamber water on the chemical diffusion gradient within the chamber. The Fe and Mn samples were analyzed in the laboratory as described above for the depth profiles of Fe and Mn.

Metal fluxes for each chamber were calculated using the following equation:

$$J = b^* \left(\frac{V}{A}\right) \tag{1}$$

where J is the flux of the soluble or total metal (mg m<sup>-2</sup> d<sup>-1</sup>), b is the slope of the line of best fit of the soluble or total metal concentrations (mg L<sup>-1</sup> d<sup>-1</sup>), V is the volume of the flux chamber (64.86 L), and A is the surface area of the flux chamber (0.27 m<sup>2</sup>).

SOD was measured as the rate at which DO depletes from the start of the experiment (hypolimnetic conditions) until DO reached <0.5 mg L<sup>-1</sup>, following USEPA (2015). SOD for each chamber in each experiment was calculated using the following equation:

$$J_{SOD} = b^* \left(\frac{V}{A}\right) \tag{2}$$

where  $J_{SOD}$  is the SOD (mg m<sup>-2</sup> d<sup>-1</sup>), b is the slope of the line of best fit of the DO concentrations (mg L<sup>-1</sup> d<sup>-1</sup>), V is the volume of the flux chamber (64.86 L), and A is the surface area of the flux chamber (0.27 m<sup>2</sup>).

#### 2.4.2. Hypolimnetic metals mass budget

We calculated the hypolimnetic Fe and Mn budget at weekly intervals from May to October 2018 to estimate Fe and Mn SWI fluxes using the following equation:

$$\frac{dM}{dt} = Q_{in}[C_{in}] - Q_{out}[C_{therm}] \pm J$$
 (3)

where  $\frac{dM}{dt}$  is the change in the hypolimnetic mass (mg d<sup>-1</sup>),  $Q_{in}$  is the flow rate of the primary tributary (L  $d^{-1}$ ),  $Q_{out}$  is the flow rate across the thermocline,  $C_{in}$  is the concentration of metals (either Fe or Mn, in mg  $L^{-1}$ ) at the inflow sampling site,  $C_{therm}$  is concentration of metals (mg  $L^{-1}$ ) at the thermocline depth and J is the estimated metal flux at the SWI (see Fig. S3 for the conceptual model of the mass balance). Positive values of I indicate that metals are released from the sediments into the water column; negative values of I indicate that metals are removed from the water column and returned to the sediments. We assumed that all water coming in from the tributary went directly to the hypolimnion because the tributary was consistently 2 °C colder than the hypolimnion (Carey et al., 2020). Additionally, we assumed that  $Q_{in} = Q_{out}$ , as there was no change in water level in the reservoir, the water treatment plant did not extract any water from the reservoir during the monitoring period and shallow groundwater wells were routinely dry in summer 2018, suggesting that shallow groundwater inputs during this period were likely small.

To calculate the entrained metal load across the thermocline, we used the metal concentration at the median depth (3.8 m; S.D. 1.7 m; range 1.6–8 m) of the thermocline for 2018. Because the metals budget was only for the hypolimnion, we did not need to account for precipitation or evaporation.

Inflow to the reservoir was measured using a rectangular weir with a notch width of 1.1 m installed at the primary inflow of FCR. An INW Aquistar PT2x pressure sensor (INW, Kirkland, WA) recorded water level at the weir every 15 min, which we used to calculate the flow rate into the reservoir, following Gerling et al. (2014):

$$Q = K * (L - 0.2 * H) * H^{1.5}$$
(4)

where Q is the flow rate ( $m^3 min^{-1}$ ), K is 110.29, a unit conversion constant, L is the crest length of the weir (m), and H is the hydraulic head (water level) behind the weir (m) (Gerling et al., 2014). We used the data to calculate an average weekly flow for each sampling week. Total and soluble samples for Fe and Mn analysis, in addition to temperature and DO measurements, were collected weekly at the inflow stream, to yield a weekly average  $C_{in}$ . To address the uncertainty in metals inputs that occurred during unsampled storm events, we also calculated fluxes assuming 50, 100 and 200% increases in inflow metal concentrations.

To calculate  $\frac{dM}{dt}$ , we first calculated the total mass of metals in the hypolimnion using the metal concentrations in samples collected from the four depths of the hypolimnion (5.0, 8.0, 6.2, and 9.0 m) multiplied by the layer volume of the depth from which they were sampled and then summed to find the total hypolimnetic metal mass. These sampling depths have been used in previous studies to reflect hypolimnetic conditions (Gerling et al. 2014, 2016; Munger et al. 2016, 2019), as we found that the DO and temperature conditions measured at the dam sampling site were representative of upstream conditions throughout the reservoir (Carey et al., 2019). Thus, although we sampled for Fe and Mn along one depth profile near the dam, our DO and temperature data along the reservoir transect support the use of this profile as representative of hypolimnion conditions throughout the reservoir.

In a similar fashion, SOD was calculated using the change of

oxygen mass in the hypolimnion  $\left(\frac{dM}{dt}\right)$ . The volume of the

hypolimnion was calculated using bathymetry data that were interpolated using kriging interpolation techniques in ArcGIS (10.5.1). The area of the SWI was taken as the 3-D surface area of the reservoir below the median thermocline (3.8 m). The layer volume was calculated as the difference between the reservoir volume at the sample depth and the reservoir volume at the sampling depth immediately below (Fig. S3).

To determine the change in metals mass each week, we subtracted the hypolimnetic mass of the preceding week, and then divided by 7 days (the period between sampling dates). To calculate the flux per unit area of the reservoir, we divided the total hypolimnetic flux (mg d $^{-1}$ ) per week by the area of the SWI (m $^2$ ) in the hypolimnion.

#### 2.4.3. Statistical analysis

We used the non-parametric Wilcoxon rank sum tests in JMP Pro 14 (SAS Institute, Cary, NC, USA) to statistically compare: 1) the benthic fluxes measured with the chamber to those estimated with mass balance and 2) the benthic chamber fluxes in June with those measured in August. Non-parametric tests were needed because of the non-independence of time series data and the unbalanced design: there were different numbers of flux estimates between the chambers and whole-reservoir mass balance as well as a different number of flux measurements collected in the June vs. August chamber experiments. Significance was set at a p-value < 0.05.

#### 3. Results

#### 3.1. DO, ORP, temperature, and pH conditions

FCR began to thermally stratify in May 2018 and remained stratified through fall turnover in late October (Fig. 2). The thermocline ranged from 1.6 to 8 m depth throughout the stratified period (median depth  $= 3.8 \text{ m} \pm 1.7 \text{ m}$ , 1 S.D.).

Within the hypolimnion, the DO concentrations were influenced by both the natural conditions of thermal stratification and the operation of the HOx system. Between late April and mid-July, volume-weighted hypolimnetic (VWH) DO concentrations were 4.7  $\pm$  0.3 mg L $^{-1}$  (Table 1) and DO near the SWI was >2 mg L $^{-1}$  (Figs. 2 and 3). Between July 19 and 30, VWH DO concentrations decreased to 1.8 mg L $^{-1}$ . After July 30, VWH DO decreased to 0.5 mg L $^{-1}$  or lower for the rest of the stratification season until turnover (Table 1).

Similar to DO, ORP measurements show that the water column was more oxidizing in the spring and early summer (Fig. 2). Although ORP generally mimicked DO patterns under oxic conditions (see Fig. S4), when DO concentrations were depleted, ORP generally continued to decline, indicating that conditions were becoming increasingly reducing. However, one exception occurred in August—September when the water column at the sedimentwater interface was fully anoxic (DO was close to 0), but ORP values increased from 100 mV to 266 mV for two weeks early

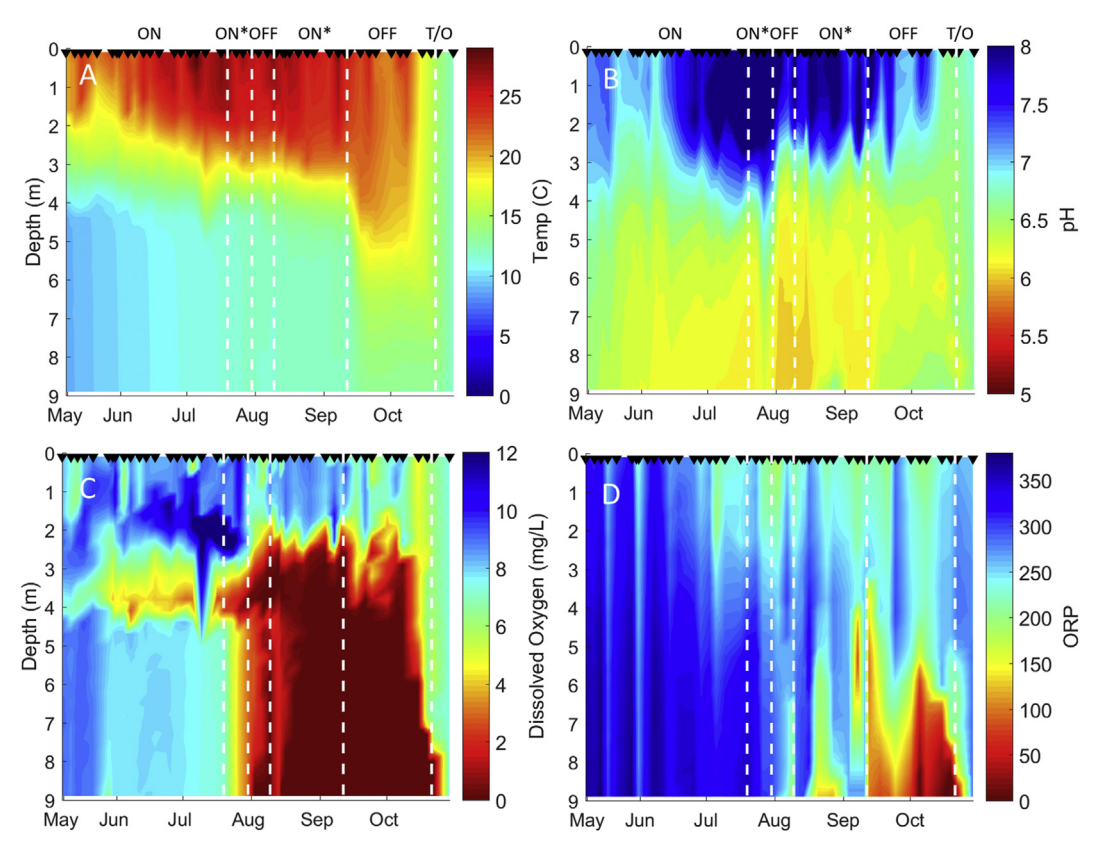


Fig. 2. Temperature (A), pH (B), dissolved oxygen (C), and oxidation-reduction potential (D; ORP) in FCR in 2018. Color scale shows concentrations or values. Dates of sampling are shown as black triangles on top of each panel; concentrations were linearly interpolated between sampling dates. Dashed vertical lines show HOx system operation at full capacity (ON), at reduced capacity (ON\*), not operational (OFF) and fall turnover (T/O; see Table 1). Full dataset published in (Carey et al., 2019). (For interpretation of the references to color in this figure legend, the reader is referred to the Web version of this article.)

# Sediment Water Interface (SWI) ON\* OFF ON\* OFF T/O ON 8 Temperature 16 Temperature (°C) 7 9 ω 9 MayJun Jul Aug Sep Oct Nov 9 ORP DO ω Ŷ

**Fig. 3.** Temperature, pH (top) and DO, ORP (bottom) at the SWI (9 m) in 2018. Dashed vertical lines show HOx system operation at full capacity (ON), at reduced capacity (ON\*), not operational (OFF) and fall turnover (T/O; see Table 1).

Sep

Oct

Nov

Aug

September before steadily decreasing to 0 mV on September 10.

The pH in the hypolimnion remained between 6 and 7 throughout the stratification period (Figs. 2 and 3). Temperature in the hypolimnion increased during the stratification period, with a peak SWI temperature of 13 °C on September 24.

# 3.2. Metal concentrations

0

May

Jun

Jul

Metal concentrations, both total and soluble forms, increased in the hypolimnion during the stratification period (Fig. 4). During the early stratified period, total and soluble concentrations were low ( $<0.5~{\rm mg~L^{-1}}$  for Fe,  $<0.05~{\rm mg~L^{-1}}$  for Mn), but began to increase during July, reaching maximum concentrations (30.9 mg L<sup>-1</sup> for total Fe and 2.7 mg L<sup>-1</sup> for total Mn) at the deepest sample point (9.0 m) in late August (Figs. 4 and 5). From September 10 to turnover on October 21, Fe and Mn concentrations were consistently elevated in the hypolimnion and were highest at the SWI. In the early part of the stratification period, total and soluble metal concentrations were similar; however, later in the season, total Fe was measurably greater than soluble Fe (Figs. 4 and 5), reflecting the presence of particulate Fe. In contrast, total Mn concentrations were similar to soluble Mn, reflecting negligible particulates.

Metal concentrations at the SWI were sensitive to ORP changes. For example, when there was a 65% increase in SWI ORP in

September (Fig. 3), total and soluble Fe concentrations at the SWI decreased 64 and 67%, respectively, while SWI total and soluble Mn decreased by 42% (Fig. 5). When ORP subsequently declined to lower values (<100 mv) in September and October, Fe and Mn concentrations at the SWI increased concomitantly (Fig. 5).

Sediment Fe and Mn concentrations in the six samples collected at the SWI near the location of the flux chambers are shown in Fig. S5. Results show that Fe concentrations ranged from 42,015 to 72,060 (mean 53,466) mg kg $^{-1}$  dry weight and Mn concentrations ranged from 347 to 897 (mean 577) mg kg $^{-1}$  dry weight. XRD analyses confirmed the presence of quartz and muscovite but did not indicate the presence of crystalline Fe or Mn mineral phases (data not shown).

#### 3.3. Benthic flux chambers

#### 3.3.1. Metal concentrations and DO/ORP conditions

Concentrations of Fe in the benthic flux chambers increased steadily over time during both incubation experiments (Fig. 6; Table S1). Total Fe concentrations reached 14 mg L<sup>-1</sup> in June and 27 mg L<sup>-1</sup> in August over a 10-day incubation. Overall, the majority  $(57 \pm 33\%)$  of total Fe in the experimental samples was composed of soluble Fe. However, there was considerable variation. At the start of the June experiment, as oxygen was depleted in the chambers, less than one-third (18-27%) of the total Fe was in soluble form, but as conditions became anoxic, the dominant form of total Fe was soluble (80-96%). During the August experiment, conditions were anoxic at the start of the experiment, and for most of the sampling intervals, the majority of Fe was in soluble form. However, there were several samples where <20% of the Fe was soluble, signifying the presence of particulate Fe. Similar to Fe, Mn concentrations increased linearly over the incubation period, reaching a maximum of 3–4 mg L<sup>-1</sup> in both the June and August experiments. In contrast to Fe, all Mn was present in soluble form.

ORP values measured during the flux chamber experiments indicate reducing conditions (Fig. 6; Table S1). In the June experiment, ORP values started at ~200 mv, indicating oxidizing conditions, but ORP decreased rapidly within the first few days, reaching 0 mv on day 4 and a low of -300 mv by the end of the experiment. Similarly, during the August experiment, ORP values started at +200 mv, but they decreased rapidly within the first day to negative values, reaching -410 mv by the end of the incubation. In both chamber experiments, ORP and DO were correlated when DO is detectable (Fig. S6); below a DO concentration of 0.5 mg  $L^{-1}$  (the lower detection limit of the sensor), ORP continued to decline, indicating the utility of measuring ORP to yield information on redox conditions. Interestingly, as ORP decreased during the experiments, it exhibited small plateaus over periods of 0.5-6 days that were often associated with sharp increases in metal concentrations. Temperature and pH remained between 12 and 15 °C and 6.3 to 7.6, respectively, throughout both experiments. For all experiments, the water column chamber measured negligible changes in soluble and total Fe and Mn concentrations (Table S1), suggesting that the reactions affecting metal cycling in the hypolimnion primarily occurred at the SWI. In addition, all or nearly all oxygen demand measured in the flux chambers can be attributed to SOD as the water column chamber measured a negligible oxygen

#### 3.3.2. Chamber metal fluxes and SOD

We calculated metal fluxes from the chamber experiments using the time series of metal concentrations (Eq (1); see data in Tables S1 and S2). Fe fluxes measured from the chamber experiments

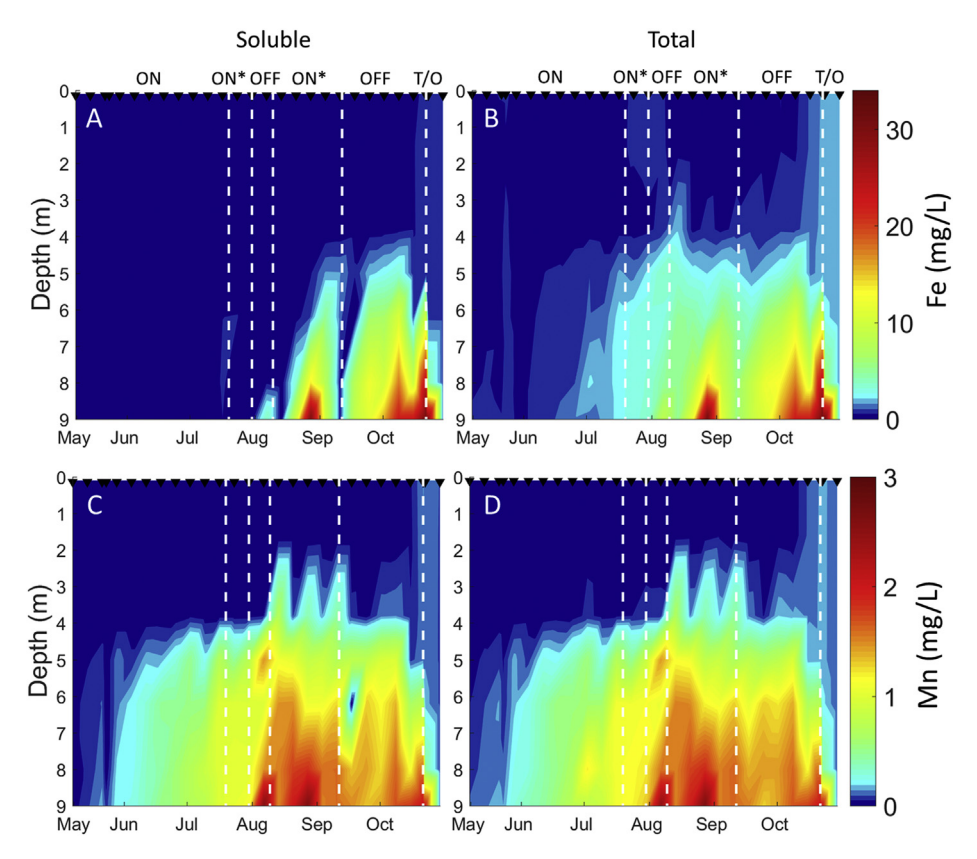


Fig. 4. Soluble (0.45 μm filtered) and total Fe (A, B) and Mn (C, D) concentrations in FCR in 2018. Color scale shows concentrations. Sampling dates shown as black triangles on top of figure; concentrations were linearly interpolated between sampling dates. Dashed vertical lines show HOx system operation at full capacity (ON), at reduced capacity (ON\*), not operational (OFF), and fall turnover (T/O; see Table 1). Full dataset is published in Schreiber et al. (2019). (For interpretation of the references to color in this figure legend, the reader is referred to the Web version of this article.)

(excluding the water column experiment) ranged from 290 to 672 mg m $^{-2}$  d $^{-1}$  (total) and 255–594 mg m $^{-2}$  d $^{-1}$  (soluble) (Fig. 7). As suggested by the wide range in measured flux values, there was considerable variability between the replicates of the flux chamber experiments, reflected by a coefficient of variation (CV) of 17% and 14% for soluble and total Fe, respectively, in June and 3% and 6% for soluble and total Fe, respectively, in August. There was no statistical difference in total or soluble Fe fluxes between the June and August experiments (Wilcoxon rank sum test:  $\chi_1^2=3.0,\,p=0.08;$  Table S3). Mn fluxes measured from the chamber experiments (excluding

Mn fluxes measured from the chamber experiments (excluding the water column experiment) ranged from 28 to 88 mg m $^{-2}$  d $^{-1}$  (total) and 29 to 89 mg m $^{-2}$  d $^{-1}$  (soluble) (Fig. 7). Similar to Fe, there was variability between replicates of the flux chamber experiments for the Mn measurements, as reflected by the coefficient of variation (CV) of 30% for both total and soluble Mn in the June experiments and 5% for both total and soluble in the August experiments. Also similar to Fe, there was no statistical difference in total or soluble Mn fluxes between the June and August experiments (Wilcoxon rank sum test:  $\chi_1^2=0.3,\ p=0.56;\ Table\ S3$ ). Almost all the Mn (98  $\pm$  0.04%) was in soluble form.

DO concentrations measured using flux chambers were used to calculate SOD (Eq (2); Fig. 7). Although the initial DO concentrations between the June and August experiments were different (VWH DO in June and August was 8 and 2 mg  $L^{-1}$ , respectively), a comparison of the two experiments showed the rate of oxygen depletion was not statistically different (Wilcoxon rank sum test:  $\chi_1^2 = 0, \, p = 1.0; \, \text{Table S3}$ ).

Fluxes of total and soluble Fe and Mn in the chamber experiments increased as sediment oxygen demand increased (i.e., became increasingly negative) (Fig. 7). Excluding one outlier for a flux chamber during the August experiment, the total and soluble Fe flux vs. SOD data fit a polynomial (quadratic) equation (p < 0.05; Table S4); the highest total and soluble Fe fluxes (672  $\pm$  51 and 594  $\pm$  128 mg m $^{-2}$  d $^{-1}$ , respectively) were measured when SOD was also the highest (1203  $\pm$  7 mg m $^{-2}$  d $^{-1}$ ). Similarly, excluding one outlier, the total and soluble Mn flux vs. SOD data fit a polynomial (quadratic) equation (p < 0.05); soluble and total Mn fluxes were highest (ranging between 35 and 37 mg m $^{-2}$  d $^{-1}$  for both total and soluble Mn) when SOD was elevated (greater than  $\sim$  450 mg m $^{-2}$  d $^{-1}$ ; Fig. 7).

#### 3.4. Hypolimnetic mass balance

#### 3.4.1. Fe and Mn loading

In the early stratification period (May–June), inflow to the reservoir was 94% higher (5.1  $\pm$  2.8 ML d $^{-1}$ ) than during July–September (0.32  $\pm$  0.44 ML d $^{-1}$ ; Fig. S7). In October, immediately before turnover, inflow was also high (4.7  $\pm$  0.4 ML d $^{-1}$ ) to the reservoir due to storms. During the May–June high inflow period, the hypolimnion experienced high input loading of metals (0.4–0.8 kg d $^{-1}$  for total Mn; 4–8 kg d $^{-1}$  for total Fe; Fig. 8A and B), but with low export of metals (~0.2 kg d $^{-1}$  for total Mn; 2–4 kg d $^{-1}$  for total Fe) across the thermocline (Fig. 8C and D). During the October high inflow period, the hypolimnion also received high input of metals, but metal export across the thermocline

### **Sediment Water Interface (SWI)**

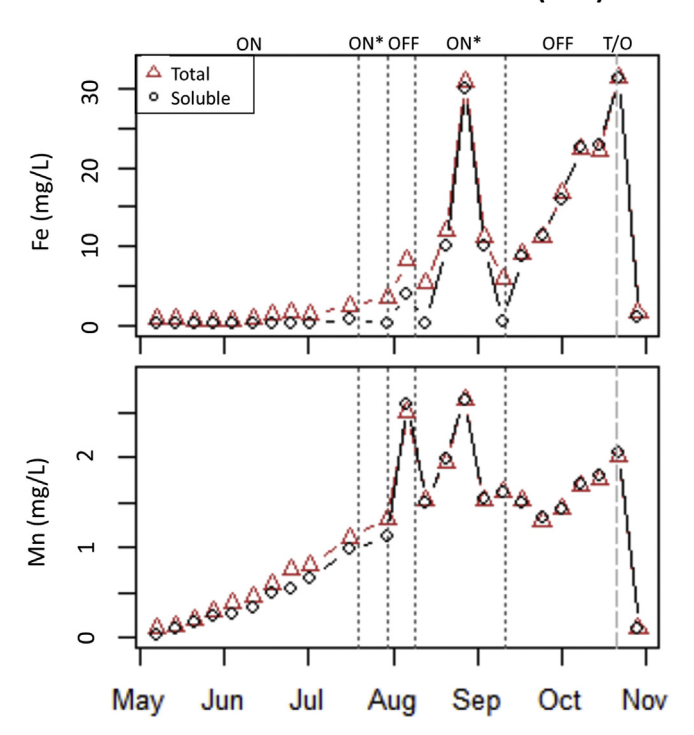


**Fig. 5.** Total and soluble (0.45  $\mu$ m filtered) Fe (top) and Mn (bottom) concentrations at the sediment-water interface (9 m) in 2018. Dashed vertical lines show HOx system operation, including at full capacity (ON), at reduced capacity (ON\*), not operational (OFF), and fall turnover (T/O; see Table 1).

downstream was substantially higher than it was in May-June.

# 3.4.2. Hypolimnetic Fe and Mn mass

The overall metal mass increased in the hypolimnion during the stratified period (Fig. 8E and F). Excluding one week in May, total Mn mass in the hypolimnion was dominated by soluble forms (73–100%) throughout the stratified period. In contrast, total Fe mass was dominated by particulate forms, especially during Julyearly September. After mid-September, more than half (41–96%) of total Fe mass was in soluble form.

#### 3.4.3. Fe and Mn fluxes between sediments and hypolimnion

Metal fluxes calculated using the mass balance (Eq (3)) were highly variable throughout the stratification period (Fig. 9). Total and soluble Fe fluxes included both positive (net release to the water column) and negative (net return to the sediment) values (-559 to  $408~mg~m^{-2}~d^{-1}$  for total Fe; -695 to  $392~mg~m^{-2}~d^{-1}$  for soluble Fe). Similarly, total and soluble Mn included positive and negative values, ranging from -96 to  $61~mg~m^{-2}~d^{-1}$  (total) and -99 to  $62~mg~m^{-2}~d^{-1}$  (soluble). Fluxes were also calculated assuming 50, 100 and 200% increases in inflow metal concentrations to account for the uncertainty of unsampled inflows during storm events. Results of these calculations (Fig. S8) show that higher metal inflow loads will result in lower positive fluxes and higher negative fluxes. However, the calculations assuming higher metals concentrations do not affect if the calculated flux is positive (release) or negative (return).

Fluxes of total and soluble Fe varied throughout the monitoring period in concert with changes in DO and ORP (Fig. 9). From May to early July, DO concentrations were generally >6 mg L<sup>-1</sup> at the SWI (ORP > 300 mV). During this time, the average total Fe flux was

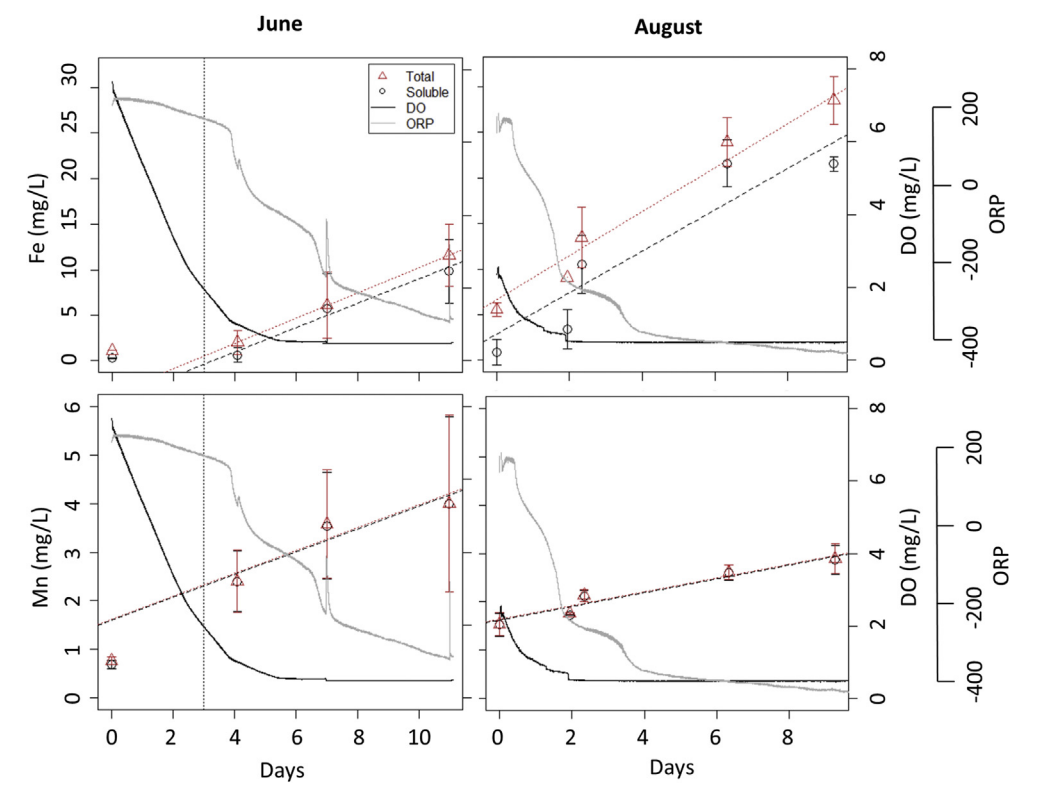
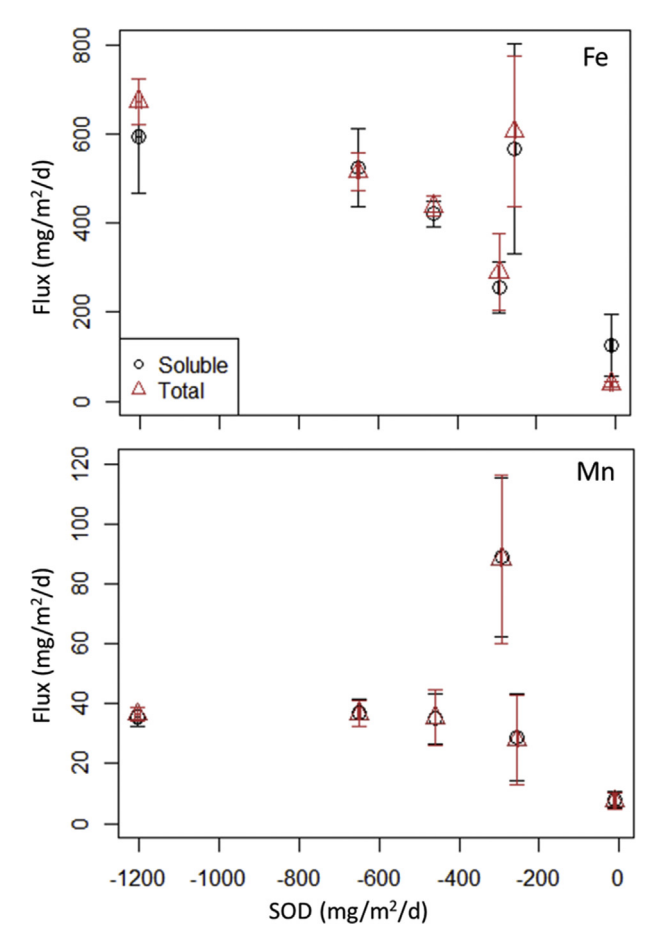


Fig. 6. Total and soluble  $(0.45 \, \mu m$  filtered) Fe and Mn concentrations (average of three chambers; error bars show one standard deviation) measured during the June (June 21-July 2, 2018) and August (August 13–23, 2018) flux chamber experiments. Data presented in Table S1. Dashed line fits show the linear regression slopes of the concentration data (see Table S2 for R2 and p-values). DO (average of three chambers) and ORP (measured in only one chamber) data collected at 2-min intervals also shown. Vertical dashed line represents the start of the June experiment, when DO  $< 2 \, \text{mg L}^{-1}$ .



**Fig. 7.** Total and soluble (0.45 μm filtered) Fe and Mn fluxes (mg m $^{-2}$  d $^{-1}$ ) measured with the flux chambers as a function of SOD (mg m $^{-2}$  d $^{-1}$ ). Results from June and August experiments (n = 5) and water column experiment (bottom right hand corner, near 0) are shown. Flux vs. SOD data, with exclusion of the outlier, were fit to a polynomial (fit data shown in Table S4). Vertical error bars reflect standard deviation of fluxes from the triplicate experiments; standard deviation of SOD was negligible.

generally negative but small (range -153 to 37, median -28 mg m $^{-2}$  d $^{-1}$ ); soluble Fe flux was close to 0 (range -16 to 12, median -0.2 mg m $^{-2}$  d $^{-1}$ ). From mid to late July, decreases in DO and ORP coincided with Fe fluxes becoming increasingly positive. On August 9, sharp but brief increases in DO and ORP, which were likely related to the reactivation of the HOx system, were associated with negative fluxes of Fe. In mid-September, when DO was fully depleted, total Fe flux was initially negative (-64 mg m $^{-2}$  d $^{-1}$ ), but shifted to positive values after one week, while soluble Fe flux quickly became positive and remained so until immediately before turnover.

Fluxes of total and soluble Mn followed similar patterns to Fe but were more variable throughout the monitoring period (Fig. 9). During the high-oxygen May to early July period, total and soluble Mn fluxes exhibited a negligible to small but positive flux (median -0.8 and 7 mg m $^{-2}$  d $^{-1}$ , respectively) from sediments into the hypolimnion. From mid-July to July 30, when VWH DO concentrations decreased to 1.8 mg L $^{-1}$ , Mn fluxes were variable, with positive fluxes occurring during times of decreasing ORP and negative fluxes occurring during times of increasing ORP (Fig. 9). Overall, as DO and ORP decreased, there was substantial release of Mn to the hypolimnion. Just as with Fe, there were negative fluxes of Mn beginning August 9, likely due to the re-activation of the HOx

system. Finally, in mid-September, coincident with a DO decrease and deactivation of the HOx system, total and soluble Mn fluxes were initially negative but became positive after one week and remained so until immediately before turnover.

After turnover (October 21), metal fluxes of both Fe and Mn were negative, reaching their maximum value for the season (up to  $-600 \text{ mg m}^{-2} \text{ d}^{-1}$  for Fe and  $-100 \text{ mg m}^{-2} \text{ d}^{-1}$  for Mn).

#### 3.5. Comparison of direct and indirect methods for estimating fluxes

Metal fluxes measured using the chambers were consistently higher than fluxes estimated using the mass balance (Fig. 10). The chamber-measured fluxes for total and soluble Fe for all experiments (n = 5; all experiments except for the water column) were 504  $\pm$  149 and 472  $\pm$  138 mg m $^{-2}$  d $^{-1}$ , respectively; in comparison, the total and soluble Fe fluxes estimated using mass balance during the same time period (n = 5) were 19  $\pm$  44 and 43  $\pm$  96 mg m $^{-2}$  d $^{-1}$ , respectively. Analysis of chamber-measured Fe fluxes to mass balance-estimated fluxes showed that they are statistically different (Wilcoxon rank sum test:  $\chi_1^2=6.8$  and p = 0.009 for both total and soluble; Table S3).

Chamber-measured fluxes for total and soluble Mn were also higher than those estimated using the mass balance (Fig. 10). The chamber-measured fluxes (n = 5; all experiments except the water column) were positive (44.9  $\pm$  25 and 45  $\pm$  25 mg m $^{-2}$  d $^{-1}$  for total and soluble Mn, respectively), while the mass balance method estimates (n = 5) during the same period were close to 0 ( $-1.9 \pm 21.4$  and  $-2.3 \pm 21$  mg m $^{-2}$  d $^{-1}$  for total and soluble Mn, respectively). Similar to Fe, statistical comparison of the chamber-measured to the mass balance fluxes showed that the two methods yielded different fluxes (Wilcoxon rank sum test:  $\chi_1^2 = 6.8$  and p = 0.009 for both total and soluble; Table S3).

#### 4. Discussion

# 4.1. Metal fluxes are highly variable and sensitive to redox conditions

Our results show that metal fluxes were highly variable over the 2018 monitoring period. Using the mass balance method, we observed negative fluxes generally under oxic conditions and positive fluxes under more reducing conditions (Fig. 9), with the switch from positive to negative fluxes coinciding with changes in DO and/or ORP. The flux chamber results support this pattern, showing that Fe and Mn fluxes increased as oxygen demand increased (Fig. 7). Higher metal release under reducing conditions and lower release under oxidizing conditions have been observed in many other studies on metal fluxes (e.g., Beutel et al., 2020; Debroux et al., 2012), but our study examined these patterns as a time-series over changing redox conditions. The rapid decrease in ORP during the flux chamber experiments reflects how quickly the redox conditions changed in the chamber over the scale of days (Fig. 6). At the start of the June experiment, ORP data combined with the metal concentration data suggest that Mn-reducing conditions dominated the volume of water/sediment enclosed by the flux chamber as there was an increase in Mn concentrations but no difference in Fe concentrations between the first two sampling points. After DO within the chamber depleted, concomitant with a decrease in ORP, our data suggest that the dominant electronaccepting process within the chamber was Fe reduction, leading to a positive Fe flux. These patterns are supported by thermodynamic predictions of terminal electron-accepting processes (e.g.,

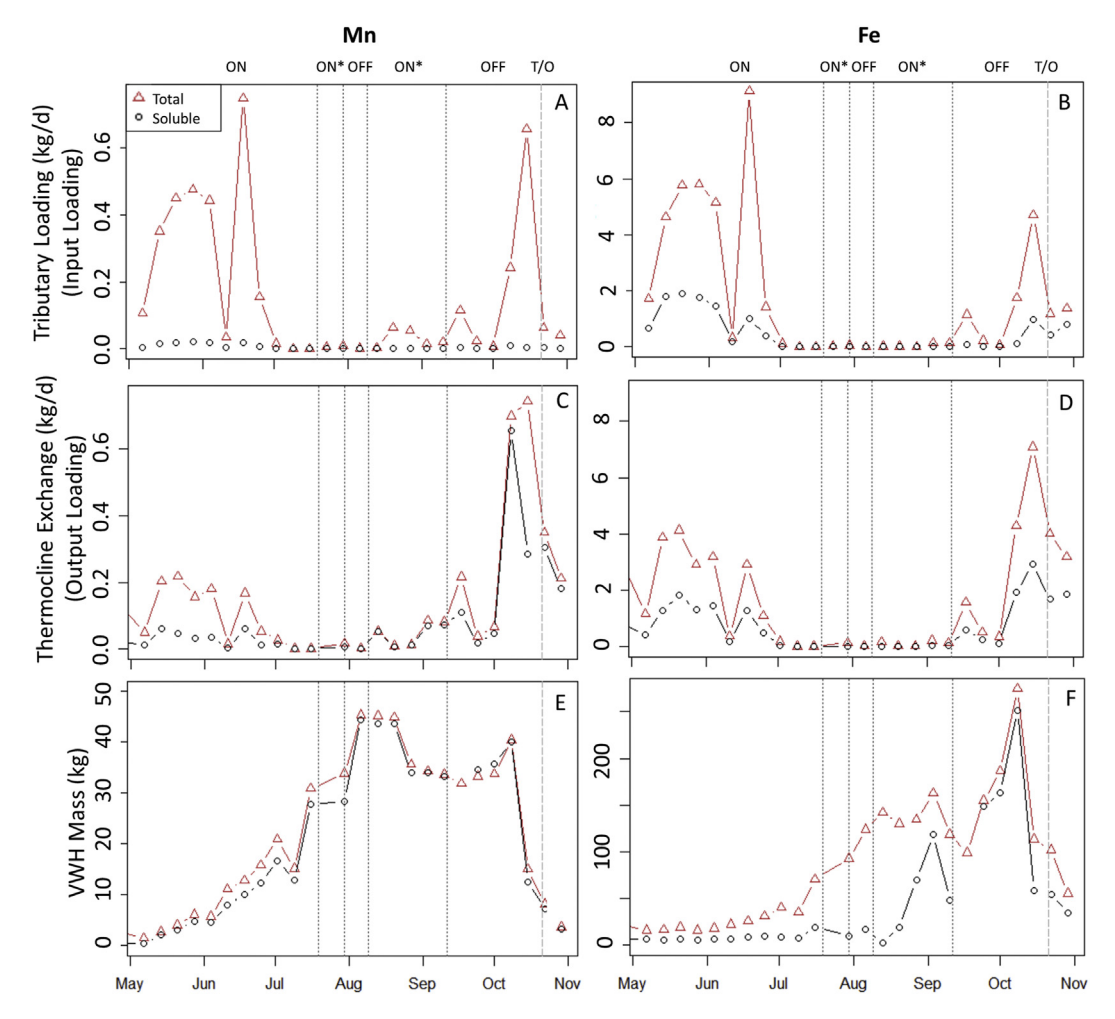


**Fig. 8.** Total and soluble (0.45 μm filtered) Mn and Fe loading via the tributary (A, B), export via thermocline exchange (C, D), and volume-weighted hypolimnetic (VWH) mass (E, F) in 2018. Dashed vertical lines show HOx system operation at full capacity (ON), at reduced capacity (ON\*), not operational (OFF) and turnover (T/O; see Table 1).

Langmuir, 1997; Stumm and Morgan, 2012 and others). In the August experiment, initial conditions within the flux chamber were more strongly reducing than in June (Fig. 6) and ORP and metals data suggest that the chamber was likely already experiencing Fereducing conditions when the experiment began. However, even under anoxic conditions, the higher concentrations of total Fe than soluble Fe (Fig. 6) suggest that Fe was being oxidized, even in the absence of DO, suggesting the presence of another oxidant, likely MnO<sub>2</sub> (De Vitre et al., 1988; Havig et al., 2015; Myers and Nealson, 1988), which can interact with Fe(II) at the sediment-water interface. Further experiments are being planned to test this idea.

The time series of metal fluxes estimated from the mass balance method also show the sensitivity of metal fluxes to changes in redox conditions (Fig. 9). Fluxes of Fe were overall negative during periods of oxidizing conditions and were positive during periods of reducing conditions. The relationship between Mn flux and redox conditions was less predictable than Fe, likely because Mn oxidation kinetics are slower than that of Fe and are less dependent on oxygen (Morgan, 2005; Munger et al., 2016); in addition, they are also strongly influenced by other biogeochemical variables, such as pH (Davison, 1993) and bacterial processes (e.g., Davison, 1993; Ghiorse, 1984; Nealson et al., 1988; Tebo et al., 2005). However, Mn fluxes were highest during ORP shifts in the water column (Fig. 9), shown by the large positive Mn flux that occurred during the steep

decline of DO/ORP in July and the sharp shift to negative Mn fluxes that occurred during the rapid increase in ORP in early September. When ORP declined on September 10 after final HOx deactivation, Fe and Mn fluxes become increasingly positive. And at turnover, fluxes became negative in response to mixing of oxic epilimnetic and anoxic hypolimnetic waters, resulting in oxidation and precipitation of metals, and a seasonal return of metals to the sediment.

The time-series changes in fluxes and relationship to redox conditions are suggestive of "hot moments", short time periods of intense biogeochemical cycling (e.g., McClain et al., 2003). Our time-series mass balance calculations were done on a weekly basis, based on our routine monitoring of water chemistry samples. However, we have other data to suggest that metal fluxes may vary on an even shorter time interval. Birgand et al. (2016) present data collected every 30-min for one week in the FCR hypolimnion using a high-frequency monitoring system, which includes a spectrophotometer connected to a multiplexor pump. Results show rapid changes in spectral data associated with Fe concentrations on a sub-daily basis, suggestive that metal fluxes may vary on hourly time scales. Further work is planned using the high-frequency monitoring system to examine metal fluxes over these short periods.

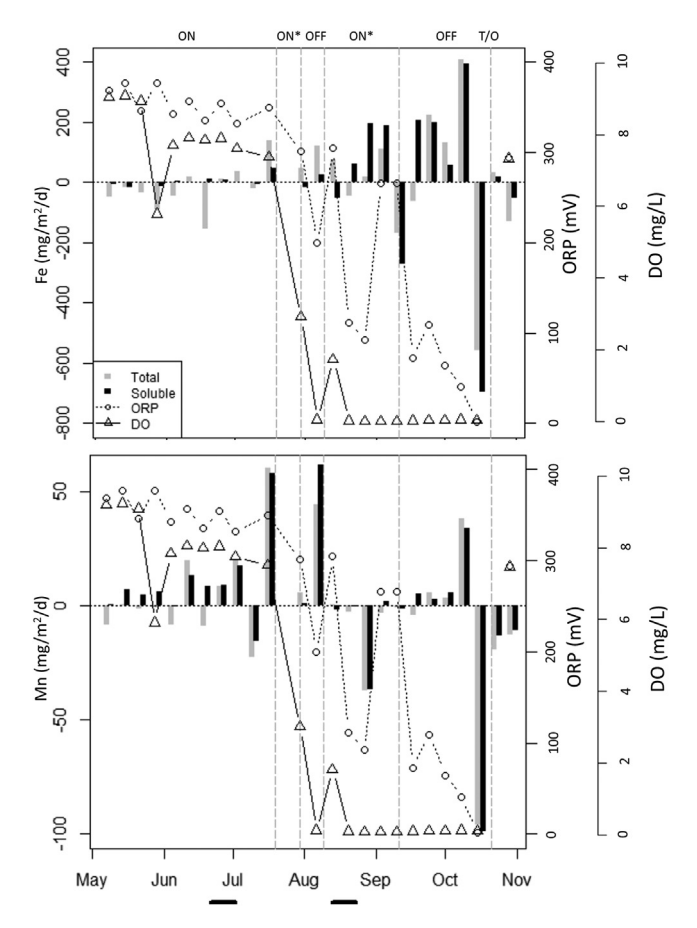


**Fig. 9.** Total and soluble (0.45  $\mu$ m filtered) Fe and Mn fluxes calculated weekly in 2018 using the mass balance method. ORP and DO at the SWI, shown on the right-hand axes, were measured weekly. Dashed vertical lines show HOx system operation at full capacity (ON), at reduced capacity (ON\*), not operational (OFF) and turnover (T/O; see Table 1). Bold horizontal lines below x-axis shows time periods of flux chamber experiments.

# 4.2. Comparison of direct and indirect methods for measuring metal fluxes

Comparison of metal fluxes measured by the flux chamber method to those estimated by mass balance show that the fluxes measured with the flux chamber were consistently higher than those calculated using the mass balance method (Fig. 10). Although previous work on phosphorous fluxes has found agreement between different methods of measuring fluxes (Nürnberg, 1987), other studies on metal fluxes have found that the flux chamber method measures the maximum metal fluxes across the SWI (Adams et al., 1982; Frogner-Kockum et al., 2016; Pakhomova et al., 2007) as the isolated chamber water does not allow for mixing with the rest of the hypolimnion. In addition, processes such as sediment resuspension and bioturbation may play a role (Pakhomova et al., 2007). In contrast, because the mass balance method relies on water column data, results are affected by mixing that can remove metals from the water column; thus flux estimates using this method will reflect minimum values (Belzile et al., 1996).

# 4.3. Comparing metal fluxes in Falling Creek Reservoir to other lakes and reservoirs

Overall, our mass balance Fe fluxes are comparable than those published in other studies on freshwater systems, while our chamber-measured Fe fluxes are typically higher (Table 2). For example, our mass balance soluble Fe fluxes over the 2018 stratification period fall within the range of fluxes measured by Belzile et al. (1996), Davison (1993), and Urban et al. (1997), but our chamber-measured soluble Fe fluxes are considerably higher. Comparison of the total Fe fluxes shows similar patterns; our mass balance total Fe flux estimates over the 2018 stratification period are within the range estimated by Brannon et al. (1985). However, our chamber estimates are substantially higher than those reported in other studies.

Unlike Fe, Mn fluxes measured in FCR, regardless of method, are comparable to fluxes measured in other studies (Table 2). Our Mn fluxes from chambers and mass balance are in the range reported by others (Belzile et al., 1996; Davison and Woof, 1984; Kawana et al., 1980; Sakata, 1985; Yagi, 1996); the only studies with substantially higher Mn fluxes were from Rostherne Mere, England (Davison and Woof, 1984) and Beppu Bay, Japan (Kawana et al., 1980).

We did not expect that our flux results would necessarily be comparable to other studies, as there are multiple variables, including different biogeochemical conditions, climate conditions, and underlying geology, amongst others, that will affect metal fluxes. This variability is one of the reasons why site-specific flux measurements are needed for quantifying metal cycles in freshwater ecosystems. For example, the Fe fluxes in Falling Creek Reservoir are likely higher than most other sites because the geologic units underlying the reservoir are crystalline rocks that contain Fe-bearing minerals including magnetite and ilmenite (Woodward, 1932). As a result of this Fe-rich bedrock, the sediment Fe concentrations at the sediment-water interface of FCR (Fig. S4; mean and S.D. of 53,467  $\pm$  11,019 mg kg<sup>-1</sup>) are elevated in comparison to 25 sediment samples collected from anoxic lakes (Nürnberg, 1995; mean and S.D. of 32,542  $\pm$  13,233 mg kg<sup>-1</sup>). In addition, as shown in Table 2, other studies used a range of methods and conducted experiments under different conditions and/or time periods. However, comparison of our data to others provides context for our results.

### 4.4. Study limitations

Both the flux chamber and the mass balance approaches have limitations as each method has its own sources of variability and uncertainty. The main source of variability in flux chamber measurements is related to the difference in replicate measurements, which is influenced by placement of the chambers and how well the chamber was sealed, in addition to site differences in sediment and pore water characteristics. Results obtained from flux chambers can also be difficult to scale up to the whole reservoir if multiple experiments are not conducted. Furthermore, like all specialized equipment, flux chamber deployments have an associated learning curve for proper deployment and operation. For example, we quickly learned that the chamber size requires the coordination of two people to deploy; however, once deployed, we were able to leave the chambers largely unattended between sampling and battery swaps. Finally, if time is restricted and only a limited number of experiments can be conducted, the flux chamber method runs the risk of low statistical strength when evaluating results.

For the mass balance method, results had inherently higher uncertainty as each variable measured had its own associated error and there are likely components of unmeasured inflow such as surface runoff and deep groundwater flow that are not considered. The use of grab samples instead of flow-proportional samples likely underestimated inflow metal loadings. In addition, the effects of the HOx system are difficult to disentangle from the high inflow

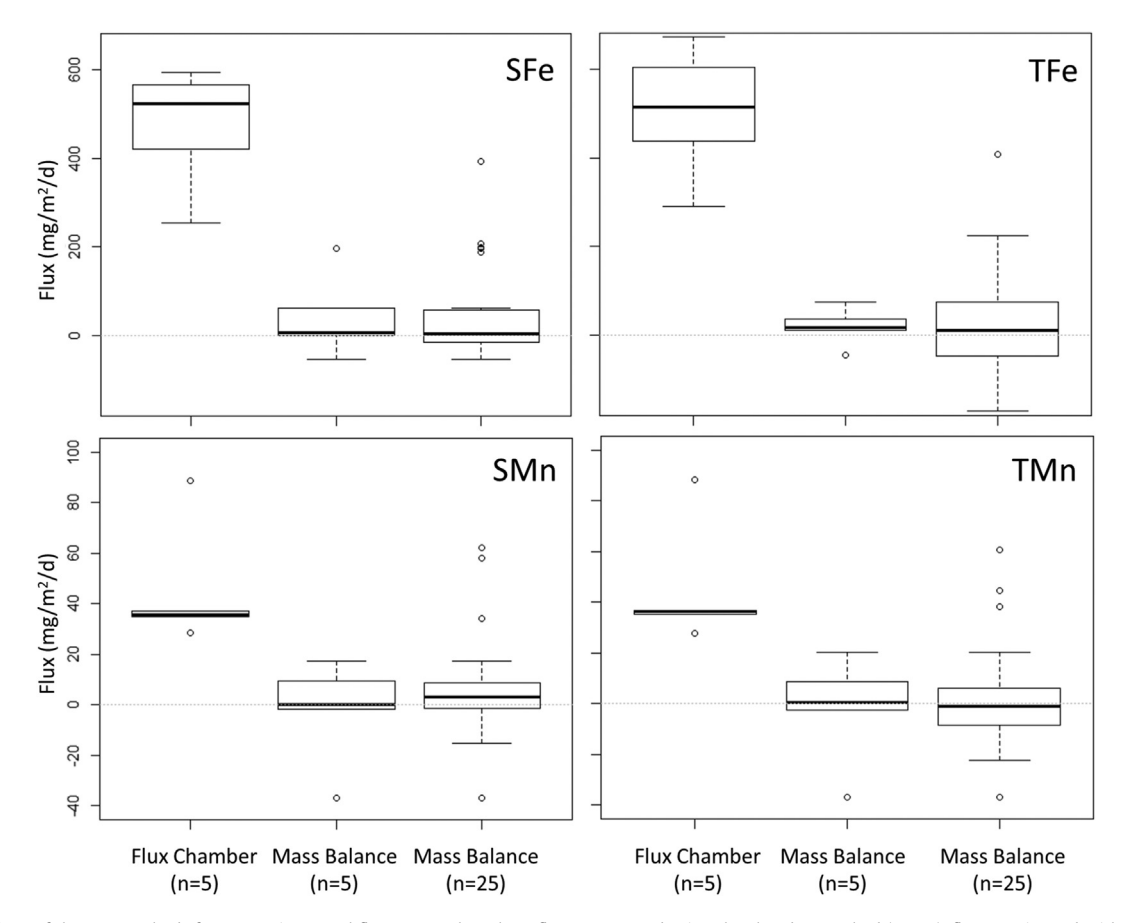


Fig. 10. Comparison of the two methods for measuring metal fluxes. Box plots show fluxes measured using the chamber method (n = 5), fluxes estimated with the mass balance method during the time periods of the chamber experiments (n = 5; see Fig. 9), and all mass balance fluxes during the 2018 stratification period (n = 25). S=Soluble (0.45  $\mu$ m filtered), T = Total.

events in the mass balance, making it hard to differentiate between hydrological and redox drivers of fluxes. Furthermore, the mass balance calculations were performed assuming one thermocline depth; however, the thermocline is variable during the stratification period as the water column continues to warm or storms entrain water downward.

Last, our study was limited in its analysis of Fe and Mn oxidation states. We used an operational definition of a 0.45  $\mu$ m filter size to differentiate total from soluble concentrations, as we have done in previous studies of metal cycling at our study site (Munger et al. 2016, 2019), but recognize that this approach does not truly reflect the Fe and Mn oxidation states in our system. We have conducted analysis of Fe(II) using the ferrozine method (Stookey, 1970) for other projects in this reservoir (data not shown); results show that soluble Fe concentrations match Fe(II) concentrations, but we have not conducted a similar analysis to distinguish Mn(II) from Mn(III) and Mn(IV) using the LBB method (Krumbein and Altmann, 1973), for example, nor were we able to analyze Fe or Mn complexes (Madison et al., 2011; Oldham et al., 2017). We plan to analyze these in future monitoring and experiments at this site to provide a more detailed analysis of metal cycling in the reservoir.

#### 5. Conclusions

The primary goal of this study was to quantify metal fluxes across the sediment-water interface into a drinking water reservoir

under different redox conditions. Overall, our results showed that metal fluxes are highly variable during the stratification period, with some periods having positive fluxes (release of metals from sediment to the water column) and some with negative fluxes (return of metals from the water column to sediment). In addition to being highly variable, the time series fluxes are highly sensitive to redox conditions in the overlying water column, suggestive of high levels of rapid metals cycling over short time periods ("hot moments"). For example, we observed rapid changes in fluxes associated with fluctuations in ORP when DO was fully depleted. These observations suggest that when the reservoir is anoxic, ORP is a useful parameter as an indicator of potential increases in metal fluxes into the water column.

Our results also show the utility of using multiple methods for estimating fluxes for quantifying the dynamics of metal exchange between sediments and the water column. Our chamber-measured fluxes provide an upper limit of metal release, an important parameter for designing HOx systems for *in-situ* treatment of metals. The mass balance fluxes, for which we have estimates for the entire stratification season, yield information on when to expect potential shifts in fluxes (release vs. return of metals), a critical parameter for predicting when additional oxygen should be added. Overall, our study suggests that use of both methods provides complementary information for evaluating Fe and Mn dynamics in reservoirs.

**Table 2**Comparison of metal fluxes and SOD from Falling Creek Reservoir to other freshwater lakes and reservoirs. If available, data are presented as ranges, means  $\pm$  standard deviation. Bolded values from Falling Creek Reservoir are from this study.

Site	Soluble Mn mg m <sup>-2</sup> d <sup>-1</sup>	Total Mn mg m <sup>-2</sup> d <sup>-1</sup>	Soluble Fe mg m <sup>-2</sup> d <sup>-1</sup>	Total Fe mg $\mathrm{m}^{-2}\mathrm{d}^{-1}$	$\begin{array}{c} \text{SOD mg m}^{-2} \\ \text{d}^{-1} \end{array}$	Temp SWI (°C)	Time of Year	Method	Location	Reference
Falling Creek Reservoir	34 (±2); 62 (±19)	34 (±2); 62 (±19)	338 (±58); 561 (±17)	364 (±52); 597 (±37)	467 (±101); 703 (±224.5)	11.5; 15	June; August	Flux Chamber	Vinton, VA, U.S.A.	This Study
T Reservoir	94					9	September	Flux Chamber	Hiroshima, Japan	Sakata (1985)
Lake Sempach			45(±34)		82(±104)		April -November	Flux Chamber	Sempach, Switzerland	Urban et al. (1997)
Falling Creek Reservoir	-99 to 62	-96 to 61	-695 to 392	-559 to 40	-226 to 519	8.8 to 13	May —October	Mass Balance	Vinton, VA, USA	This Study
Lake Fukami-ike	2						April -September	Mass Balance	Central Japan	Yagi (1996)
Lake Bret	7		20			~8	July -October	Mass Balance; Peepers	Vaud, Switzerland	Belzile et al. (1996)
Lake Mendota	18-32; 4-79					12 to 14	July–Sept; Sept–Oct	Water Chemistry	Madison, WI, USA	(Stauffer, 1986)
Esthwaite Water			10 to 190				•	Water Chemistry	Lake District, England	Davison (1993)
Rostherne Mere	126; 66					7 to 8	June; October	Water Chemistry	Cheshire, England	Davison and Woof (1984)
Beppu Bay	126					11 to 12		Water	Japan	Kawana et al. (1980)
Jinpen Reservoir	4 to 14		~0.5 to 4			5 to 30	November	Peepers	Northwest China	(Li et al., 2019)
Lake Sempach	110 11		19 (±17)		9 (±4)	5 10 50	April -November	Peepers	Sempach, Switzerland	Urban et al. (1997)
Lake Bret	1		13				July -October	Peepers	Vaud, Switzerland	Belzile et al. (1996)
Carvins Cove Reservoir	19–37				25.6 (±40) to 258 (±37)		June; August	Peepers	Roanoke, VA, USA	Bryant et al. (2011)
Red Rock Reservoir; DeGray Reservoir		39 (±5); 10 (±4)		66 (±15); 34 (±10)				Experimental Incubation	Marion Co., IA; Clark Co., AR, USA	Brannon et al. (1985)
Hodges Reservoir		36, 63		(=10)	2000		March		San Diego, CA	Beutel et al. (2020)
Deer Lake		10 to 28		3.4 to 9.0		10	October		Spokane, WA	(Beutel et al., 2008)
Lake Bard		2 to 5			150 to 210; 480 to 550	14	July		Thousand Oaks CA	,

#### Data availability

Data shown in Fig. 2 are available in the Environmental Data Initiative (EDI) repository (Carey et al., 2019).

Data shown in Fig. 4 are available in the Environmental Data Initiative (EDI) repository (Schreiber et al., 2019).

#### **Declaration of competing interest**

The authors declare that they have no known competing financial interests or personal relationships that could have appeared to influence the work reported in this paper.

#### Acknowledgements

This work has been supported by the Virginia Tech Institute for Critical Technology and Applied Science, the Virginia Tech Department of Geosciences, the Consortium of University for the Advancement of Hydrologic Science, Inc, the Virginia Tech Graduate Student Assembly, the Virginia Water Resources Research Center, the Geological Society of America, and the National Science Foundation (CNS-1737424, DEB-1753639, REU-1659495). We gratefully acknowledge the Western Virginia Water Authority for allowing us access to the reservoir to conduct these experiments, Athena Tilley for ICP-AES analysis, Jeff Parks for ICP-MS analysis and Neil Johnson for XRD analysis. We also thank Bethany Bookout for field support and John Chermak for advice about practical applications of this work. We thank the reviewers and the editor for their insightful comments that greatly improved the manuscript. Last but not least, we greatly appreciate numerous discussions with the late Don

Rimstidt about metal geochemistry, to whom we dedicate this work.

# Appendix A. Supplementary information

Supplementary information for this article can be found online at https://doi.org/10.1016/j.watres.2020.116003.

### References

Adams, D.D., Matisoff, G., Snodgrass, W.J., 1982. Flux of reduced chemical constituents (Fe<sup>2+</sup>, Mn<sup>2+</sup>, NH<sup>+</sup><sub>4</sub>and CH<sub>4</sub>) and sediment oxygen demand in Lake Erie. Hydrobiologia 91, 405–414, 0.

AWWA, 2009. Inorganics Committee Report: a survey of the "other" inorganics. Journal - AWWA 101 (8), 79–86.

Belzile, N., Pizarro, J., Filella, M., Buffle, J., 1996. Sediment diffusive fluxes of Fe, Mn, and P in a eutrophic lake: contribution from lateral vs bottom sediments. Aquat. Sci. 58 (4), 327–354.

Beutel, M., Fuhrmann, B., Herbon, G., Chow, A., Brower, S., Pasek, J., 2020. Cycling of methylmercury and other redox-sensitive compounds in the profundal zone of a hypereutrophic water supply reservoir. Hydrobiologia 1–22.

Beutel, M.W., 2003. Hypolimnetic anoxia and sediment oxygen demand in California drinking water reservoirs. Lake Reservoir Manag. 19 (3), 208–221.

Beutel, M.W., Horne, A.J., 1999. A review of the effects of hypolimnetic oxygenation on lake and reservoir water quality. Lake Reservoir Manag. 15 (4), 285–297.

Beutel, M.W., Leonard, T.M., Dent, S.R., Moore, B.C., 2008. Effects of aerobic and anaerobic conditions on P, N, Fe, Mn, and Hg accumulation in waters overlaying profundal sediments of an oligo-mesotrophic lake. Water Res. 42 (8), 1953–1962.

Bierlein, K.A., Rezvani, M., Socolofsky, S.A., Bryant, L.D., Wüest, A., Little, J.C., 2017. Increased sediment oxygen flux in lakes and reservoirs: the impact of hypolimnetic oxygenation. Water Resour. Res. 53 (6), 4876–4890.

Birgand, F., Aveni-Deforge, K., Smith, B., Maxwell, B., Horstman, M., Gerling, A.B.,
Carey, C.C., 2016. First report of a novel multiplexer pumping system coupled to
a water quality probe to collect high temporal frequency in situ water chemistry
measurements at multiple sites. Limnol Oceanogr. Methods 14 (12), 767–783.
Bouchard, M., Laforest, F., Vandelac, L., Bellinger, D., Mergler, D., 2007. Hair

- manganese and hyperactive behaviors: pilot study of school-age children exposed through tap water. Environ. Health Perspect. 115 (1), 122–127.
- Bouchard, M.F., Sauvé, S., Barbeau, B., Legrand, M., Brodeur, M.-È., Bouffard, T., Limoges, E., Bellinger, D.C., Mergler, D., 2011. Intellectual impairment in schoolage children exposed to manganese from drinking water. Environ. Health Perspect. 119 (1), 138–143.
- Brannon, J.M., Chen, R.L., Gunnison, D., 1985. Sediment-water interactions and mineral cycling in reservoirs. In: Gunnison, D. (Ed.), Microbial Processes in Reservoirs. Springer Netherlands, Dordrecht, pp. 121–134.
- Bryant, L.D., Hsu-Kim, H., Gantzer, P.A., Little, J.C., 2011. Solving the problem at the source: controlling Mn release at the sediment-water interface via hypolimnetic oxygenation. Water Res. 45 (19), 6381–6392.
- Carey, C.C., Hounshell, A.G., Lofton, M.E., Bookout, B.J., Corrigan, R.S., Gerling, A.B., McClure, R.P., Woelmer, W.M., 2020. Discharge time series for the primary inflow tributary entering Falling Creek Reservoir, Vinton, Virginia, USA 2013-2020 ver 6. Environ. Data Initiative. https://doi.org/10.6073/pasta/30caad87e3e5aafd1f9ace836c94d2fa.
- Carey, C.C., McClure, R.P., Gerling, A.B., Doubek, J.P., Chen, S., Lofton, M.E., Hamre, K.D., 2019. Time series of high-frequency profiles of depth, temperature, dissolved oxygen, conductivity, specific conductivity, chlorophyll a, turbidity, pH, oxidation-reduction potential, photosynthetic active radiation, and descent rate for Beaverdam Reservoir, Carvins Cove Reservoir, Falling Creek Reservoir, Gatewood Reservoir, and Spring Hollow Reservoir in Southwestern Virginia, USA 2013-2018., Environ. Data Initiative. https://doi.org/10.6073/pasta/1fc7d2a5c69c6a651793dba06d375ae2.
- Davison, W., 1993. Iron and manganese in lakes. Earth Sci. Rev. 34 (2), 119-163.
- Davison, W., Woof, C., 1984. A study of the cycling of manganese and other elements in a seasonally anoxic lake, Rostherne Mere, UK. Water Res. 18 (6), 727–734.
- De Vitre, R., Buffle, J., Perret, D., Baudat, R., 1988. A study of iron and manganese transformations at the O<sub>2</sub>S(-II) transition layer in a eutrophic lake (Lake Bret, Switzerland): a multimethod approach. Geochem. Cosmochim. Acta 52 (6), 1601–1613.
- Debroux, J.-F., Beutel, M.W., Thompson, C.M., Mulligan, S., 2012. Design and testing of a novel hypolimnetic oxygenation system to improve water quality in Lake Bard, California. Lake Reservoir Manag. 28 (3), 245–254.
- Di Toro, D.M., Connolly, J.P., 1980. Mathematical Models of Water Quality in Large Lakes Part 2: Lake Erie, P. 249, USEPA. Environmental Research Laboratory, Office of Research and Development, Duluth, MN.
- Frogner-Kockum, P., Göransson, P., Åslund, H., Ländell, M., Stevens, R., Tengberg, A., Göransson, G., Ohlsson, Y., 2016. Metal contaminant fluxes across the sediment water interface. Mar. Pollut. Bull. 111 (1–2), 321–329.
- Gantzer, P.A., Bryant, L.D., Little, J.C., 2009. Controlling soluble iron and manganese in a water-supply reservoir using hypolimnetic oxygenation. Water Res. 43 (5), 1285–1294.
- Gerling, A.B., Browne, R.G., Gantzer, P.A., Mobley, M.H., Little, J.C., Carey, C.C., 2014. First report of the successful operation of a side stream supersaturation hypolimnetic oxygenation system in a eutrophic, shallow reservoir. Water Res. 67, 129–143.
- Gerling, A.B., Munger, Z.W., Doubek, J.P., Hamre, K.D., Gantzer, P.A., Little, J.C., Carey, C.C., 2016. Whole-catchment manipulations of internal and external loading reveal the sensitivity of a century-old reservoir to hypoxia. Ecosystems 19 (3), 555–571.
- Ghiorse, W., 1984. Biology of iron- and manganese-depositing bacteria. Annu. Rev. Microbiol. 38 (1), 515–550.
- Havig, J.R., McCormick, M.L., Hamilton, T.L., Kump, L.R., 2015. The behavior of biologically important trace elements across the oxic/euxinic transition of meromictic Fayetteville Green Lake, New York, USA. Geochem. Cosmochim. Acta 165, 389–406.
- Hicks, D., 1990. Environmental Protection Agency Region IV Perspective on SOD. In: Proceedings: US Army Corps of Engineers Workshop on Sediment Oxygen Demand. U.S. Army Corps of Engineers, pp. 110–119.
- Kawana, K., Shiozawa, T., Hoshika, A., Tanimoto, T., Takimura, O., 1980. Diffusion of manganese from bottom sediments in Beppu Bay. La Mer 18 (3), 131–137.
- Khan, K., Factor-Litvak, P., Wasserman, G., Liu, X., Ahmed, E., Parvez, F., Slavkovich, V., Levy, D., Mey, J., van Geen, A., Graziano, J., 2011. Manganese exposure from drinking water and children's classroom behavior in Bangladesh. Environ. Health Perspect. 119 (10), 1501–1506.
- Krumbein, W., Altmann, H., 1973. A new method for the detection and enumeration of manganese oxidizing and reducing microorganisms. Helgoländer Wissenschaftliche Meeresuntersuchungen 25 (2), 347.
- Langmuir, D., 1997. Aqueous Environmental Geochemistry. Prentice Hall, Upper Saddle River, NJ.
- Li, N., Huang, T., Mao, X., Zhang, H., Li, K., Wen, G., Lv, X., Deng, L., 2019. Controlling reduced iron and manganese in a drinking water reservoir by hypolimnetic aeration and artificial destratification. Sci. Total Environ. 685, 497–507.
- Madison, A.S., Tebo, B.M., Luther III, G.W., 2011. Simultaneous determination of soluble manganese (III), manganese (II) and total manganese in natural (pore) waters. Talanta 84 (2), 374–381.
- McClain, M.E., Boyer, E.W., Dent, C.L., Gergel, S.E., Grimm, N.B., Groffman, P.M., Hart, S.C., Harvey, J.W., Johnston, C.A., Mayorga, E., 2003. Biogeochemical hot spots and hot moments at the interface of terrestrial and aquatic ecosystems. Ecosystems 301—312.
- Morgan, J.J., 2005. Kinetics of reaction between  $O_2$  and Mn (II) species in aqueous solutions. Geochem. Cosmochim. Acta 69 (1), 35–48.
- Munger, Z.W., Carey, C.C., Gerling, A.B., Doubek, J.P., Hamre, K.D., McClure, R.P., Schreiber, M.E., 2019. Oxygenation and hydrologic controls on iron and

- manganese mass budgets in a drinking-water reservoir. Lake Reservoir Manag. 35 (3), 277–291.
- Munger, Z.W., Carey, C.C., Gerling, A.B., Hamre, K.D., Doubek, J.P., Klepatzki, S.D., McClure, R.P., Schreiber, M.E., 2016. Effectiveness of hypolimnetic oxygenation for preventing accumulation of Fe and Mn in a drinking water reservoir. Water Res. 106. 1–14.
- Murphy, P.J., Hicks, D.B., 1986. In-situ method for measuring sediment oxygen demand. In: Hatcher, K. (Ed.), Sediment Oxygen Demand: Processes, Modeling, and Measurement. Institute of Natural Resources, University of Georgia, Athens, Georgia, pp. 307–323.
- Myers, C.R., Nealson, K.H., 1988. Microbial reduction of manganese oxides: interactions with iron and sulfur. Geochem. Cosmochim. Acta 52 (11), 2727–2732.
- Nealson, K.H., Tebo, B.M., Rosson, R.A., 1988. Occurrence and mechanisms of microbial oxidation of manganese. Advances in Applied Microbiology. Elsevier, pp. 279–318.
- Nürnberg, G.K., 1987. A comparison of internal phosphorus loads in lakes with anoxic hypolimnia: laboratory incubation versus in situ hypolimnetic phosphorus accumulation 1. Limnol. Oceanogr. 32 (5), 1160–1164.
- Nürnberg, G.K., 1995. Quantifying anoxia in lakes. Limnol. Oceanogr. 40 (6), 1100–1111.
- Oldham, V.E., Mucci, A., Tebo, B.M., Luther III, G.W., 2017. Soluble Mn (III)—L complexes are abundant in oxygenated waters and stabilized by humic ligands. Geochem. Cosmochim. Acta 199, 238—246.
- Pais, I., Jones, J.B., 1997. The Handbook of Trace Elements. Taylor & Francis.
- Pakhomova, S.V., Hall, P.O., Kononets, M.Y., Rozanov, A.G., Tengberg, A., Vershinin, A.V., 2007. Fluxes of iron and manganese across the sediment—water interface under various redox conditions. Mar. Chem. 107 (3), 319–331.
- Polak, J., Haffner, D., 1978. Oxygen depletion of Hamilton Harbour. Water Res. 12 (4), 205–215.
- Preece, E.P., Moore, B.C., Skinner, M.M., Child, A., Dent, S., 2019. A review of the biological and chemical effects of hypolimnetic oxygenation. Lake Reservoir Manag. 35 (3), 229–246.
- Read, J.S., Hamilton, D.P., Jones, I.D., Muraoka, K., Winslow, L.A., Kroiss, R., Wu, C.H., Gaiser, E., 2011. Derivation of lake mixing and stratification indices from highresolution lake buoy data. Environ. Model. Software 26 (11), 1325–1336.
- Sakata, M., 1985. Diagenetic remobilization of manganese, iron, copper and lead in anoxic sediment of a freshwater pond. Water Res. 19 (8), 1033–1038.
- Schreiber, M.E., Krueger, K.M., Munger, Z.W., Hammond, N.W., Lofton, M.E., McClure, R.P., Carey, C.C., 2019. Metals Data from Falling Creek Reservoir and Beaverdam Reservoir from 2014 to 2019. Environmental Data Initiative. https://doi.org/10.6073/pasta/a44de21f9da5d6f62d110b45251d4242.
- Stauffer, R.E., 1986. Cycling of manganese and iron in Lake Mendota, Wisconsin. Environ. Sci. Technol. 20 (5), 449–457.
- Stookey, L.L., 1970. Ferrozine—a new spectrophotometric reagent for iron. Anal. Chem. 42 (7), 779—781.
- Stumm, W., Morgan, J.J., 2012. Aquatic Chemistry: Chemical Equilibria and Rates in Natural Waters, third ed. John Wiley & Sons.
- Tebo, B.M., Johnson, H.A., McCarthy, J.K., Templeton, A.S., 2005. Geomicrobiology of manganese (II) oxidation. Trends Microbiol. 13 (9), 421–428.
- Tengberg, A., Hall, P.O.J., Andersson, U., Lindén, B., Styrenius, O., Boland, G., de Bovee, F., Carlsson, B., Ceradini, S., Devol, A., Duineveld, G., Friemann, J.U., Glud, R.N., Khripounoff, A., Leather, J., Linke, P., Lund-Hansen, L., Rowe, G., Santschi, P., de Wilde, P., Witte, U., 2005. Intercalibration of benthic flux chambers: II. Hydrodynamic characterization and flux comparisons of 14 different designs. Mar. Chem. 94 (1), 147–173.
- Urban, N.R., Dinkel, C., Wehrli, B., 1997. Solute transfer across the sediment surface of a eutrophic lake: I. Porewater profiles from dialysis samplers. Aquat. Sci. 59 (1), 1–25.
- USEPA, 1994. Method 200.7: Determination of Metals and Trace Elements in Water and Wastes by Inductively Coupled Plasma-Atomic Emission Spectrometry. ORD, Environmental Monitoring Systems Lab, Cincinnati.
- USEPA, 2003. Health Effects Support Document for Manganese. EPA 822-R-03-003, Washington DC.
- USEPA, 2007. Method 3051A (SW-846): Microwave Assisted Acid Digestion of Sediments, Sludges, and Soils. Environmental Protection Agency, Washington, DC. USA.
- USEPA, 2015. Operating Procedure: Sediment Oxygen Demand. USEPA Region 4 Science and Ecosystem Support Division, Athens, GA.
- USEPA, 2017. Secondary drinking water standards: guidance for nuisance chemicals. https://www.epa.gov/dwstandardsregulations/secondary-drinking-water-standards-guidance-nuisance-chemicals.
- Walker, R.R., Snodgrass, W.J., 1986. Model for sediment oxygen demand in lakes. J. Environ. Eng. 112 (1), 25–43.
- Wasserman, G.A., Liu, X., Parvez, F., Factor-Litvak, P., Ahsan, H., Levy, D., Kline, J., van Geen, A., Mey, J., Slavkovich, V., Siddique, A.B., Islam, T., Graziano, J.H., 2011. Arsenic and manganese exposure and children's intellectual function. Neurotoxicology 32 (4), 450–457.
- Wetzel, R.G., 2001. Limnology: Lake and River Ecosystems, third ed. Academic Press. WHO, 2008. Guidelines for Drinking-Water Quality. World Health Organization, Geneva, Switzerland.
- Woodward, H.P., 1932. Geology and Mineral Resources of the Roanoke Area. Virginia, Virginia Geological Survey, Richmond, VA.
- Yagi, A., 1996. Manganese flux associated with dissolved and suspended manganese forms in Lake Fukami-ike. Water Res. 30 (8), 1823–1832.
- Zaw, M., Chiswell, B., 1999. Iron and manganese dynamics in lake water. Water Res. 33 (8), 1900–1910.